Published in final edited form as:
Radiat Res. 2011 June ; 175(6): 774–783. doi:10.1667/RR2214.1.

Localized CT-Guided Irradiation Inhibits Neurogenesis in Specific Regions of the Adult Mouse Brain

E. C. Ford[a,1], **P. Achanta**[c], **D. Purger**[c], **M. Armour**[a], **J. Reyes**[a], **J. Fong**[a], **L. Kleinberg**[a], **K. Redmond**[a], **J. Wong**[a], **M. H. Jang**[d,e], **H. Jun**[d], **H-J. Song**[d,e,f], and **A. Quinones-Hinojosa**[b,c]

[a] Department of Radiation Oncology and Molecular Radiation Sciences, The Johns Hopkins University School of Medicine, Baltimore, Maryland [b] Department of Oncology, The Johns Hopkins University School of Medicine, Baltimore, Maryland [c] Department of Neurosurgery, The Johns Hopkins University School of Medicine, Baltimore, Maryland [d] Institute for Cell Engineering, The Johns Hopkins University School of Medicine, Baltimore, Maryland [e] Department of Neurology, The Johns Hopkins University School of Medicine, Baltimore, Maryland [f] Department of Neuroscience, The Johns Hopkins University School of Medicine, Baltimore, Maryland

Abstract

Radiation is used in the study of neurogenesis in the adult mouse both as a model for patients undergoing radiation therapy for CNS malignancies and as a tool to interrupt neurogenesis. We describe the use of a dedicated CT-guided precision device to irradiate specific sub-regions of the adult mouse brain. Improved CT visualization was accomplished with intrathecal injection of iodinated contrast agent, which enhances the lateral ventricles. T2-weighted MRI images were also used for target localization. Visualization of delivered beams (10 Gy) in tissue was accomplished with immunohistochemical staining for the protein γ-H2AX, a marker of DNA double-strand breaks. γ-H2AX stains showed that the lateral ventricle wall could be targeted with an accuracy of 0.19 mm (n = 10). In the hippocampus, γ-H2AX staining showed that the dentate gyrus can be irradiated unilaterally with a localized arc treatment. This resulted in a significant decrease of proliferative neural progenitor cells as measured by Ki-67 staining ($P < 0.001$) while leaving the contralateral side intact. Two months after localized irradiation, neurogenesis was significantly inhibited in the irradiated region as seen with EdU/NeuN double labeling ($P < 0.001$). Localized radiation in the rodent brain is a promising new tool for the study of neurogenesis.

INTRODUCTION

Radiation is known to strongly affect the birth and differentiation of new neurons, and it has therefore been used as a laboratory tool in the study of neurogenesis (1–3). In rodent models two specific neurogenic niches are known: the subventricular zone (SVZ) of the lateral wall of the lateral ventricle and the subgranular zone (SGZ) of the dentate gyrus of the hippocampus (4–8). Radiation has been used to selectively inhibit the birth of new neurons in the mouse SGZ. For example, using radiation to suppress neurogenesis, Santarelli *et al.* showed that neurogenesis is required for the behavioral benefits of two classes of antidepressants (9). Similar radiation-suppression studies by our group and collaborators have examined the effect of a selective serotonin reuptake inhibitor, sertraline, in a mouse

[1]Address for correspondence: Department of Radiation Oncology and Molecular Radiation Sciences, Johns Hopkins University, 401 North Broadway, Suite 1440, Baltimore, MD 21231; eric.ford@jhmi.edu.

model of Huntington's disease. The ability of sertraline to arrest disease progression was shown to be dependent on neurogenesis (10). More generally, a variety of radiation studies have examined the effect of arrested neurogenesis in the SGZ on behavioral end points (11–20). The effect of radiation on neurogenesis in the SVZ has also been explored (21–25). This neurogenic niche is particularly powerful as a model to study migration of neural progenitor cells (26).

In addition to the study of neurogenesis, rodent models of CNS irradiation are relevant to clinical oncology since radiation is a widely used component of the definitive management of patients with brain tumors. Finally, the effects of radiation exposure on the brain and cognition are believed to be an ultimate limitation on long-term human space travel, and rodent models are an important tool for understanding and mitigating these effects (18, 27).

Most of the data collected to date have relied on technology limited to irradiation of the majority or entirety of the rodent brain. However, efforts are currently under way to develop a technology that is similar to that used in modern radiation therapy clinics by providing radiation delivery that is highly localized in small animals (28–34). Radiation beams as small as 0.5 mm have been used (28), but the full realization of this potential requires precise end-to-end calibration of the device (35).

Here we investigate the capabilities of our newly developed radiation device for precision irradiation of the mouse brain. We outline a technique to provide enhanced CT contrast in the brain and describe a method for visualizing the radiation dose distribution directly in tissue using immunohistochemical staining for γ-H2AX, a marker of DNA double-strand breaks. The use of this novel device for irradiation of neurogenic niches may have a significant implication in the study of stem cells in the mammalian brain.

MATERIALS AND METHODS

Subjects

All experiments described in this study were performed with the approval of the Johns Hopkins Animal Care and Use Committee under standard animal care and use protocols. Studies were performed on 6–8-week-old male C57BL6/J mice.

The Small Animal Radiation Research Platform (SARRP)

The SARRP is a precision radiation device capable of delivering of radiation beams down to 0.5 mm in diameter under CT guidance (28). It consists of a dual source X-ray tube attached to a gantry that rotates over a range of 120° (Fig. 1). A flat-panel detector (Perkin-Elmer, ANS1040) is used to acquire images when the gantry is in the horizontal position. For this study, CT images were reconstructed with an isotropic voxel size of 0.20 mm. For imaging we operated the tube with a 0.4-mm focal spot, beam energy of 100 kVp and 1 mm Al filtration. For treatment we operated the tube at 225 kVp, a 3-mm focal spot and filtration of 0.25 mm Cu + 1 mm Al.

On-board CT imaging allowed the identification of a target while the animal is in the treatment position. The target was localized using the XVI CT navigation software (Netherlands Cancer Institute, NKI, Amsterdam). After localization on CT, the animal was moved to the appropriate treatment location by the robotic positioner which has four degrees of freedom (X, Y, Z, θ). Through a combination of gantry and robot stage angles, beams can be delivered from nearly any direction relative to the animal, and stereotactic arc-like treatments are possible. For these and all other imaging studies, the mice were positioned in a custom head holder that is CT and MRI compatible as described by Armour *et al.* (36).

The total time required to treat a mouse (from animal setup to completion of beam delivery) was approximately 10 min for a 10-Gy treatment with a 3 × 3-mm beam.

The mechanical calibration of the system is critical to ensuring that beams from various angles all intersect in a single point. Calibration was accomplished with a semi-automatic imaging-based method, where end-to-end alignment accuracy has been measured to be 0.2 mm (35). To test this calibration, we measured dose distributions with GAFchromic films embedded in a water-equivalent plastic phantom (37).

Intrathecal Iodine Contrast Agent

To enhance CT-based tissue visualization for brain applications, we have developed a technique of intrathecal iodine contrast. The technique is based on a previous method of blood or saline injection into the cisterna magna to study subarachnoid hemorrhages (38). In our approach, we exposed the cisterna magna by moving aside three layers of muscle in the back of the neck in a sterile procedure performed under analgesia and anesthesia with the injection of 90 mg/kg ketamine + 20 mg/kg xylazine intraperitoneally. An iodine contrast medium, Iohexol 300 mgI/ml (GE Inc., Oslo, Norway), was injected under the dura mater, the thin membrane layer covering the cisterna magna using a 30-gauge needle on a 1-ml syringe. Injected volumes were 50 μl for a 13–20-g mouse and 70 μl for a 20–30-g mouse, which had been determined empirically to be non-toxic. The injection was performed with the aid of a microscope to ensure that the vessels lining the dorsal surface of the medulla were not ruptured. The needle was held in place for 1 min to prevent backflow. Mice that undergo this procedure survive long term; our longest time thus far is 2 months after injection. No signs of infection or neurological deficit have been observed in over 200 mice in various experiments. Repeat CT scans were performed over 100 min postinjection to determine the time course of contrast washout. The washout kinetics was quantified by measuring the contrast-to-noise ratio in the CT scans. Least-squares non-linear fitting was performed in Matlab v.7.1.0 (Math-works Inc., Natick, MA) using the functional form: $1 + C_0 \cdot \exp(-ln2 \cdot t/t_h)$.

MR-Based Targeting

As an aid to target localization, we performed an MRI scan of a mouse on a 9.4 T unit (Bruker Inc., Billerica, MA) using a T2-weighted sequence (TR = 4000 ms, TE = 25 ms) for visualization of the ventricles and other soft tissue landmarks. Scan acquisition time was approximately 8 min with this sequence for 40 slices. The hippocampus was clearly visualized. The MR image was co-registered with the SARRP CT using the navigation software. For this application, the same structure is visible in CT and MRI (i.e. lateral ventricles), so the accuracy of CT-MRI registration is expected to be similar to a CT-CT registration accuracy of 0.5 mm (standard deviation in vector shift) as measured by Armour *et al.* (36). For the experiments conducted here, the MRI scans were acquired as an adjunct, but the intrathecal iodine contrast scan was used for radiation targeting.

Brain Irradiation

Radiation was delivered to a mouse using the SARRP with anesthesia administered as described above. Intrathecal iodine injection was performed as described above followed by CT acquisition on the SARRP platform. The first set of experiments was done to validate targeting of the radiation beam. The target was the right lateral wall of the right lateral ventricle identified using the CT navigation software and automatically imported into the robot positioning interface. The appropriate collimator and filtration were attached and radiation was delivered. The second set of experiments aimed to demonstrate local irradiation of the hippocampus. A T2-weighted MRI scan previously acquired on a 9.4 T unit (Bruker Inc., Billerica, MA) was used for targeting. The MRI was co-registered with the

SARRP CT based on the location of the lateral ventricles, and the dentate gyrus was targeted.

Immunohistochemistry

Brains were harvested after transcardial perfusion first with 0.9% saline, then 4% paraformaldehyde (PFA) performed under deep anesthesia. The tissue was post-fixed for 8 h in PFA followed by a sink in 30% sucrose and then an overnight soaking in Tissue-Tek OCT Compound (Sakura, Torrance, CA) at 4°C. Finally the tissue was frozen in OCT. Cyrosectioning of coronal slices was performed with 10-, 30- or 40-μm slice thickness as noted below.

Staining of sections consisted of antigen retrieval with sodium citrate (0.01 *M* in deionized water), rinse in phosphate-buffered saline (PBS, 3 × 5 min), 1 h incubation in blocking serum (10% goat serum with 0.1% Triton X-100 for membrane permeabilization), overnight incubation at 4°C in primary antibody (as specified below), PBS rinse (3 × 5 min), 1 h incubation in secondary antibody (1:500 goat anti-mouse or goat anti-rabbit Alexa Fluor 488 conjugated, Millipore, Inc.), PBS rinse (3 × 5 min), DAPI counterstain 5 min (1:200 in deionized water), PBS rinse (2 × 5 min), dry and mount. Sections were visualized using a fluorescence microscope (Olympus Inc.).

The first data set consisted of immunohistochemical staining of γ-H2AX, the H2AX histone protein that is phosphorylated after DNA double-strand breaks. γ-H2AX has been widely used in brain and other tissues (39–43), and the number of γ-H2AX$^+$ foci appears to correlate well with radiation dose over a wide range of doses (44). The timing is important because the γ-H2AX signal is lost after DNA repair, a process that begins almost immediately after irradiation. Mice were euthanized 1 h after irradiation and tissue was sectioned into 10-μm-thick sections. A primary anti-mouse antibody for phospho-histone H2AX Ser139 (Millipore, Inc.) in 1:700 dilution was used.

To quantify targeting accuracy, we measured the location of the center of the radiation beam in γ-H2AX-stained sections using the digital readout of the microscope. We then measured the location of the right edge of the right lateral ventricle (the intended target) and calculated the offset between these two locations. We performed these measurements on 10 mice irradiated on 2 different days. Two coronal sections each were collected at a rostral-caudal aspect that was anatomically consistent with the visualization of the beam isocenter on CT.

To assess cellular proliferation, we employed staining of Ki-67, a protein present in every phase of the cell cycle except G_0 that is widely used to study proliferating cells in the brain and their responses to radiation (45, 46). In this experiment three mice were euthanized 24 h after irradiation and tissue was processed as outlined above using 30-μm-thick sections. A rabbit monoclonal anti-Ki-67 (Neomarkers, Inc.) primary antibody was used in a 1:500 dilution. The quantification of Ki-67$^+$ cells in the subgranular zone of the dentate gyrus was performed by stereological counting on three mice using 40-μm tissue sections evenly spaced along the entire rostral-caudal length of the dentate gyrus. Images were acquired on a Zeiss LSM 510 Live confocal system (Carl Zeiss). Cell counting was performed in every fifth section, and the results are reported as the number of cells per unit volume of tissue (no./mm^3).

To quantify the effect of localized radiation on neurogenesis, we conducted an experiment using pulse labeling with EdU, a nucleoside analog that is incorporated into the DNA during the S phase of the cell cycle (47, 48). Radiation (10 Gy) was delivered in a conformal arc treatment targeting the dentate gyrus of the right hippocampus of three mice as described above. Beginning 4 weeks after irradiation, we injected EdU (50 mg/kg once per day for 5

days). Mice were euthanized 4 weeks after the first EdU injection. Coronal brain sections (40 μm thick) were prepared and processed for immuno-staining using anti-NeuN antibodies (Chemicon; 1:300) and EdU (Invitrogen) as described previously (49). Images were acquired on a Zeiss LSM 510 Live confocal system (Carl Zeiss). Stereological quantification of $EdU^+/NeuN^+$ cells in the subgranular zone and granule cell layer was carried out as described previously (47).

RESULTS

CT and MR-Based Targeting and Accuracy

CT-based targeting for brain applications is enhanced by the injection of intrathecal iodine contrast. The contrast is clearly visualized in the lateral ventricles in CT scans acquired on the SARRP (Fig. 2A, B). The contrast washes out with a half-life of 19 min (Fig. 2C). T2-weighted MRI images clearly show both the lateral ventricles and the hippocampus structure (Fig. 3). These MRI images can be overlaid with the CT scan for targeting purposes.

Once the CT-based target is defined, the accuracy of the system calibration is critical for ensuring that all radiation beams are delivered precisely to the target point. Figure 4 shows end-to-end test results from an arc treatment with the 1-mm-diameter beam using GAF-chromic films in a phantom. The gantry was set at an angle with respect to the phantom while the robotic stage was rotated, generating an ‘‘arc’’ or cone of radiation. Here two arcs were delivered with the gantry at two separate gantry angles of 60° and 30° from the vertical. The full width at half maximum (FWHM) is 2.31 mm, which is larger than 1.0 mm since the arcs impinge on the film at an angle. Theoretically the beam size at this angle should be 2.0 mm. The well-localized beam spot shown in Fig. 4 demonstrates the good alignment of beams from different directions.

Beam Targeting Validation with γ-H2AX

To further explore the possibility of visualizing the actual beam in tissue, a 1-mm-diameter beam was delivered to the right lateral cortex and striatum. Resultant γ-H2AX staining allowed clear visualization of the beam (Fig. 5). To quantify the targeting accuracy of the beam in a realistic experimental scenario, we delivered a 3 × 3-mm square beam to the lateral wall of the lateral ventricle as visualized on intrathecal contrast enhanced CT. Resultant γ-H2AX staining showed precise targeting of the expected location (Fig. 6). The beam edge is also extremely sharp, in agreement with film-based physics commissioning measurements that indicate a 20–80% penumbra of 0.3 mm (50). We measured the distance between the intended target (lateral ventricle wall) and the center of the beam as visualized in the tissue sections. The center of the beam was offset from the lateral wall by a mean distance of 0.16 ± 0.31 mm (standard deviation) in the 10 irradiated mice.

To include the effect of tissue shrinkage during fixing, freezing and processing, we measured the width of the beam on the histological sections. The mean beam width was 2.63 ± 0.10 mm. Since the actual width of the beam is known to be precisely 3.1 mm based on commissioning physics measurements for this setup (50), the tissue shrank by a factor of 0.85. Applying this scaling factor to the above measurement for beam offset, we found that the actual beam offset was 0.19 ± 0.36 mm. Similarly, the scaled beam width in Fig. 6 is 3.0 mm and the offset of the beam from the lateral wall is 0.10 mm.

In the final experiment, we delivered radiation specifically to the right hippocampus with a stereotac-tic-like arc treatment consisting of two arcs at 45° and 30° from the vertical. Targeting was CT-based using a co-registered T2-weighted MRI to enhance visualization. The γ-H2AX signal was well localized to the right dentate gyrus (Fig. 7), while no positive cells were observed on the contralateral side. The tissue dorsal to the hippocampus shows γ-

H2AX staining since the radiation beams enter through this region and also possibly because of enhancement by the overlaying bone even though a relatively hard X-ray beam is used (225 kVp, 0.25 mm Cu filtration). The green signal in the ventral and contralateral regions is non-specific staining and at high magnification does not co-localize with the DAPI signal. The bright line in the right lateral side is due to a tissue fold.

Ki-67 Quantification

Figure 8 shows representative Ki-67 IHC stains from the right dentate gyrus in an unirradiated (panel A) and irradiated mouse (panel B). There is a marked decrease in the number of Ki-67$^+$ cells on the irradiated side. Figure 8C shows the results of stereological quantification from this experiment. There is a factor of 3.5 decrease in the density of Ki-67$^+$ cells in the right side for an unirradiated mouse compared to an irradiated mouse, and this difference is highly significant ($P = 0.001$). None of the other differences are significant, neither the left side for sham-irradiated compared to irradiated ($P = 0.11$) nor the right side (irradiated) compared to left side (unirradiated) in the irradiated mice ($P = 0.06$). Data are tabulated in Table 1.

Neurogenesis

In irradiated mice the number of cells incorporating EdU at 4 weeks after treatment is significantly reduced (Fig. 9C). The number of EdU$^+$ cells on the irradiated side is reduced to 3.4 times that in unirradiated mice, and this reduction is significant ($P = 0.012$). The number of EdU$^+$ cells that become NeuN$^+$ cells 8 weeks after irradiation is also significantly reduced (Fig. 9D). The number of EdU$^+$/NeuN$^+$ cells is reduced to 8.5 times that in unirradiated mice ($P = 0.001$). On the unirradiated (left) side, there were no significant differences from animals that received no treatment in either the number of EdU$^+$ cells at 4 weeks ($P = 0.52$) or the number of EdU$^+$/NeuN$^+$ cells at eight weeks ($P = 0.71$). Data are tabulated in Table 1.

DISCUSSION

We demonstrate the delivery of highly localized beams of radiation to the mouse brain. Using on-board CT guidance we found that the beam could be located within 0.19 mm of the intended target as determined by immunohistochemical staining with γ-H2AX. Using an arc delivery technique we are able to deliver radiation to a small volume of tissue (approximately 1% of the total brain volume), in this case to the hippocampus. We show that using this technique cellular proliferation is interrupted at early times and that at late times after irradiation, the generation of new neurons is reduced.

The effects of radiation doses below 10 Gy on the rodent brain have been widely studied (2, 3, 9, 10, 13, 14, 18, 21–25, 46, 51–56) as a model system for damage incurred from radiotherapy for brain tumors and also as a means of interrupting neurogenesis. In the absence of radiation, proliferating cells in the SVZ and SGZ develop into new neurons with an approximate efficiency of 80% (53). Delivery of radiation at doses as low as 2 Gy has been shown to suppress cellular proliferation in both the SVZ (24) and SGZ (57). These effects last long-term, with one recent study showing inhibited proliferation for more than 15 months after 25 Gy (23). The ability of radiation to suppress neurogenesis can be used in a variety of ways. For example, it can be used to study effects of neurogenesis on various behavioral end points, (3) or to assess the role of neurogenesis in the action of particular pharmaceutical agents (9).

Previous studies have commonly used whole-brain or whole-body irradiation. A common concern with such techniques is possible confounding factors involved in the irradiation of

large volumes of brain tissue, though to our knowledge there has been no study that directly compares the effects of whole-brain irradiation with localized irradiation in the rodent. To avoid possible confounding effects, some groups have attempted to target the radiation to specific regions of the brain. Santarelli *et al.* and others, for example, used 3.2 × 11-mm collimators to irradiate the hippocampus (9, 14, 17). Other similar approaches have been reported using either custom shields (1, 22, 23) or, in one case, the 4-mm collimator of the Gamma Knife device for rats (13). Recently, Kiehl *et al.* demonstrated hemispherical brain irradiation of the mouse with a collimated ^{192}Ir source coupled with computerized treatment planning (30). One challenge with these approaches is that on-board CT is generally not available, which is critical to obtain the accuracy achieved here (36). A second challenge is that in some systems where a high-energy ^{192}Ir or ^{60}Co beam is used (15, 18, 48, 49), the beam edges will be blurred due to the larger range of high-energy secondary electrons in tissue. Our γ-H2AX results show relatively sharp beam edges, which are a result of the small focal spot and relatively low-energy X rays (225 kVp). Commissioning measurements indicate that for a 1-mm beam, the dose at 2 mm off-axis is only 0.5% of the on-axis value (50).

One possible limitation of the immunohistochemical approach to validate targeting outlined here is the need for tissue processing promptly after irradiation. Numerous reports have investigated the dependence of the γ-H2AX signal on radiation dose and time after irradiation (41, 43, 44). The γ-H2AX signal is gradually eliminated through DNA repair processes, following similar kinetics to the resolution of ATM foci (61). Though some signal may be present at late times as has been observed in other terminally differentiated cell lines (40), the strength of the γ-H2AX staining may limit this technique to early times, which means that one may not be able to use tissue from the same animals that are used for experiments at later times.

The data on cellular proliferation is interesting since is well known that the proliferating cells in the dentate gyrus are neural progenitor cells (45, 58–60). It is interesting to compare our results to those of Mizumatsu *et al.* (46), who also used Ki-67 staining to quantify radiation-induced changes in proliferation in the hippocampus of the same strain of mice. Our stereology approaches differ, so the absolute numbers are difficult to compare. However, Mizumatsu *et al.* found a >10-fold reduction in Ki-67$^+$ cells after a dose of 10 Gy whereas we found an approximately 3-fold reduction. This could be due to the time considered (48 or 24 h). However, we note that the reduction of EdU incorporation at 4 weeks after irradiation is also reduced by approximately a factor of 3 compared to unirradiated animals. The difference compared to previous results could also be due to the manner in which the radiation is delivered. Perhaps localized irradiation results in less of a reduction in proliferating cells. This may be consistent with the data of Santarelli *et al.* (9), who delivered a localized form of radiation to approximately one-third of the brain to a dose of 5 Gy × 3. That study noted a reduction of approximately 5-fold in the number of BrdU$^+$ cells in the hippocampal subgranular zone. Further work is required to determine the source of such differences.

Our neurogenesis study demonstrates that localized irradiation also reduces neurogenesis long term. One month after localized irradiation, there are significantly reduced numbers of proliferating cells in the irradiated region as seen with EdU staining. The proliferating cells that do remain are capable of differentiating into new neurons, as seen with EdU/NeuN double labeling, but there are many fewer young neurons generated in the irradiated region. This is consistent with the previous studies cited above that showed that neurogenesis was strongly inhibited after irradiation. However, those studies employed much more extensive radiation fields encompassing large portions of the brain (2, 46, 53). In our experiments the high-dose radiation region is restricted to a volume of tissue that is approximately 1% of the

total brain volume and yet neurogenesis is still inhibited. This calls into question the hypothesis that neurogenic inhibition is due to the accumulation of activated microglia and the related increase in pro-inflammatory cytokines (53). It is unlikely that irradiation of such small fields would lead to such a strong inflammatory response that lasted for months, but further work is needed for validation.

CONCLUSIONS

Numerous previous studies have employed radiation to interrupt neurogenesis in the hippocampus or the SVZ (2, 3, 9, 10, 13, 14, 18, 21–25, 46, 51–56). Here we show that it is possible to irradiate specific sub-regions within these structures to control the precise location where neurogenic ablation occurs. The immunohistochemical validation data presented here show that, with this system, the radiation beam can be positioned to within less than a millimeter of the intended target. Our novel radiation platform is a powerful tool to study stem cell niches in the mammalian brain, and localized ablation may prove an important tool in future studies of neurogenesis.

Acknowledgments

We acknowledge laboratory funding from the National Institutes of Health, NCI grant no. R01CA108449 (ECF and JW), NINDS grant no. K08NS055851 (AQH), no. R01NS047344 (HJS), NIA grant no. R01AG024984 (HJS), NIMH grant no. K99MH090115 (MHJ), the Robert Wood Johnson Foundation (AQH and PA), the James S. McDonnell Foundation (AQH and PA), the Maryland Stem Cell Research Fund (AQH and DP) and the Howard Hughes Medical Institute (AQH and DP). We thank Dr. Rafael Tamargo and Eric Momin for assistance in learning the techniques of intrathecal injections. We thank the SARRP engineering development team of Peter Kazanzides, Iulian Iordachita and Babak Matinfar for continued support on the system. We thank Woody Armour for helpful discussions. There is a technology transfer agreement between Johns Hopkins University and Gulmay Inc. (Surrey, UK). JW is the PI on a Research Service Agreement with Gulmay Inc. to provide continued refinement of the system.

References

1. Fike JR, Rola R, Limoli CL. Radiation response of neural precursor cells. Neurosurg Clin N Am. 2007; 18:115–127. [PubMed: 17244559]
2. Monje ML, Mizumatsu S, Fike JR, Palmer TD. Irradiation induces neural precursor-cell dysfunction. Nat Med. 2002; 8:955–962. [PubMed: 12161748]
3. Wojtowicz JM. Irradiation as an experimental tool in studies of adult neurogenesis. Hippocampus. 2006; 16:261–266. [PubMed: 16435311]
4. Lois C, Alvarez-Buylla A. Proliferating subventricular zone cells in the adult mammalian forebrain can differentiate into neurons and glia. Proc Natl Acad Sci USA. 1993; 90:2074–2077. [PubMed: 8446631]
5. Alvarez-Buylla A, García-Verdugo JM. Neurogenesis in adult subventricular zone. J Neurosci. 2002; 22:629–634. [PubMed: 11826091]
6. Quinones-Hinojosa A, Sanai N, Soriano-Navarro M, Gonzalez-Perez O, Mirzadeh Z, Gil-Perotin S, Romero-Rodriguez R, Berger MS, Garcia-Verdugo JM, Alvarez-Buylla A. Cellular composition and cytoarchitecture of the adult human subventricular zone: A niche of neural stem cells. J Comp Neurol. 2006; 494:415–434. [PubMed: 16320258]
7. Quinones-Hinojosa A, Chaichana K. The human subventricular zone: A source of new cells and a potential source of brain tumors. Exp Neurol. 2007; 205:313–324. [PubMed: 17459377]
8. Ming GL, Song H. Adult neurogenesis in the mammalian central nervous system. Annu Rev Neurosci. 2005; 28:223–250. [PubMed: 16022595]
9. Santarelli L, Saxe M, Gross C, Surget A, Battaglia F, Dulawa S, Weisstaub N, Lee J, Duman R, Hen R. Requirement of hippocampal neurogenesis for the behavioral effects of antidepressants. Science. 2003; 301:805–809. [PubMed: 12907793]

10. Duan W, Peng Q, Masuda N, Ford E, Tryggestad E, Ladenheim B, Zhao M, Cadet JL, Wong J, Ross CA. Sertraline slows disease progression and increases neurogenesis in N171-82Q mouse model of huntington's disease. Neurobiol Dis. 2008; 30:312–322. [PubMed: 18403212]
11. Hernández-Rabaza V, Llorens-Martín M, Velázquez-Sánchez C, Ferragud A, Arcusa A, Gumus HG, Gómez-Pinedo U, Pérez-Villalba A, Roselló J, Canales JJ. Inhibition of adult hippocampal neurogenesis disrupts contextual learning but spares spatial working memory, long-term conditional rule retention and spatial reversal. Neuroscience. 2009; 159:59–68. [PubMed: 19138728]
12. Clark PJ, Brzezinska WJ, Thomas MW, Ryzhenko NA, Toshkov SA, Rhodes JS. Intact neurogenesis is required for benefits of exercise on spatial memory but not motor performance or contextual fear conditioning in C57BL/6J mice. Neuroscience. 2008; 155:1048–1058. [PubMed: 18664375]
13. Saxe MD, Battaglia F, Wang JW, Malleret G, David DJ, Monckton JE, Garcia ADR, Sofroniew MV, Kandel ER, Drew MR. Ablation of hippocampal neurogenesis impairs contextual fear conditioning and synaptic plasticity in the dentate gyrus. Proc Natl Acad Sci USA. 2006; 103:17501–17506. [PubMed: 17088541]
14. Meshi D, Drew MR, Saxe M, Ansorge MS, David D, Santarelli L, Malapani C, Moore H, Hen R. Hippocampal neurogenesis is not required for behavioral effects of environmental enrichment. Nat Neurosci. 2006; 9:729–731. [PubMed: 16648847]
15. Winocur G, Wojtowicz JM, Sekeres M, Snyder JS, Wang S. Inhibition of neurogenesis interferes with hippocampus-dependent memory function. Hippocampus. 2006; 16:296–304. [PubMed: 16411241]
16. Raber J, Fan Y, Matsumori Y, Liu Z, Weinstein PR, Fike JR, Liu J. Irradiation attenuates neurogenesis and exacerbates ischemia-induced deficits. Ann Neurol. 2004; 55:381–389. [PubMed: 14991816]
17. Raber J, Rola R, LeFevour A, Morhardt D, Curley J, Mizumatsu S, VandenBerg SR, Fike JR. Radiation-induced cognitive impairments are associated with changes in indicators of hippocampal neurogenesis. Radiat Res. 2004; 162:39–47. [PubMed: 15222778]
18. Rola R, Raber J, Rizk A, Otsuka S, VandenBerg SR, Morhardt DR, Fike JR. Radiation-induced impairment of hippocampal neurogenesis is associated with cognitive deficits in young mice. Exp Neurol. 2004; 188:316–330. [PubMed: 15246832]
19. Madsen TM, Kristjansen PEG, Bolwig TG, Wörtwein G. Arrested neuronal proliferation and impaired hippocampal function following fractionated brain irradiation in the adult rat. Neuroscience. 2003; 119:635–642. [PubMed: 12809684]
20. Shors TJ, Townsend DA, Zhao M, Kozorovitskiy Y, Gould E. Neurogenesis may relate to some but not all types of hippocampal-dependent learning. Hippocampus. 2002; 12:578–584. [PubMed: 12440573]
21. Hellström NA, Björk-Eriksson T, Blomgren K, Kuhn HG. Differential recovery of neural stem cells in the subventricular zone and dentate gyrus after ionizing radiation. Stem Cells. 2009; 27:634–641. [PubMed: 19056908]
22. McGinn MJ, Sun D, Colello RJ. Utilizing X-irradiation to selectively eliminate neural stem/progenitor cells from neurogenic regions of the mammalian brain. J Neurosci Methods. 2008; 170:9–15. [PubMed: 18280577]
23. Panagiotakos G, Alshamy G, Chan B, Abrams R, Greenberg E, Saxena A, Bradbury M, Edgar M, Gutin P, Tabar V. Long-term impact of radiation on the stem cell and oligodendrocyte precursors in the brain. PLoS One. 2007; 2:e588. [PubMed: 17622341]
24. Tada E, Yang C, Gobbel GT, Lamborn KR, Fike JR. Long-term impairment of subependymal repopulation following damage by ionizing irradiation. Exp Neurol. 1999; 160:66–77. [PubMed: 10630191]
25. Shinohara C, Gobbel GT, Lamborn KR, Tada E, Fike JR. Apoptosis in the subependyma of young adult rats after single and fractionated doses of X-rays. Cancer Res. 1997; 57:2694–2702. [PubMed: 9205079]
26. Lois C, Alvarez-Buylla A. Long-distance neuronal migration in the adult mammalian brain. Science. 1994; 264:1145–1148. [PubMed: 8178174]

27. Setlow RB. The U.S. National Research Council's views of the radiation hazards in space. Mutat Res. 1999; 430:169–175. [PubMed: 10631330]
28. Wong J, Armour E, Kazanzides P, Iordachita I, Tryggestad E, Deng H, Matinfar M, Kennedy C, Liu Z, DeWeese TL. High-resolution, small animal radiation research platform with X-ray tomographic guidance capabilities. Int J Radiat Oncol Biol Phys. 2008; 71:1591–1599. [PubMed: 18640502]
29. Lindsay P, Ansell S, Moseley DJ, Jelveh S, Hill R, Jaffray D. Development of an image-guided conformal small animal irradiation platform. J Med Phys. 2008; 35:2695.
30. Kiehl EL, Stojadinovic S, Malinowski KT, Limbrick D, Jost SC, Garbow JR, Rubin JB, Deasy JO, Khullar D, Hope AJ. Feasibility of small animal cranial irradiation with the microRT system. Med Phys. 2008; 35:4735–4743. [PubMed: 18975718]
31. Wang S, Liu Z, Sultana S, Schreiber E, Zhou O, Chang S. A novel high resolution micro-radiotherapy system for small animal irradiation for cancer research. Biofactors. 2007; 30:265–270. [PubMed: 18607076]
32. Stojadinovic S, Low DA, Hope AJ, Vicic M, Deasy JO, Cui J, Khullar D, Parikh PJ, Malinowski KT, Grigsby PW. MicroRT-small animal conformal irradiator. Med Phys. 2007; 34:4706–4716. [PubMed: 18196798]
33. Graves EE, Zhou H, Chatterjee R, Keall PJ, Gambhir SS, Contag CH, Boyer AL. Design and evaluation of a variable aperture collimator for conformal radiotherapy of small animals using a microCT scanner. Med Phys. 2007; 34:4359–4367. [PubMed: 18072501]
34. Stojadinovic S, Low DA, Vicic M, Mutic S, Deasy JO, Hope AJ, Parikh PJ, Grigsby PW. Progress toward a microradiation therapy small animal conformal irradiator. Med Phys. 2006; 33:3834–3845. [PubMed: 17089848]
35. Matinfar M, Ford E, Iordachita I, Wong J, Kazanzides P. Image-guided small animal radiation research platform: Calibration of treatment beam alignment. Phys Med Biol. 2009; 54:891–905. [PubMed: 19141881]
36. Armour M, Ford E, Iordachita I, Wong J. CT guidance is needed to achieve reproducible positioning of the mouse head for repeat precision cranial irradiation. Radiat Res. 2010; 173:119–123. [PubMed: 20041766]
37. Deng H, Kennedy CW, Armour E, Tryggestad E, Ford E, McNutt T, Jiang L, Wong J. The small-animal radiation research platform (SARRP): Dosimetry of a focused lens system. Phys Med Biol. 2007; 52:2729–2740. [PubMed: 17473348]
38. Chaichana KL, Levy AP, Miller-Lotan R, Shakur S, Tamargo RJ. Haptoglobin 2-2 genotype determines chronic vasospasm after experimental subarachnoid hemorrhage. Stroke. 2007; 38:3266–3271. [PubMed: 17962599]
39. Short SC, Martindale C, Bourne S, Brand G, Woodcock M, Johnston P. DNA repair after irradiation in glioma cells and normal human astrocytes. Neuro Oncol. 2007; 9:404–411. [PubMed: 17704360]
40. Gavrilov B, Vezhenkova I, Firsanov D, Solovjeva L, Svetlova M, Mikhailov V, Tomilin N. Slow elimination of phosphorylated histone γ-H2AX from DNA of terminally differentiated mouse heart cells in situ. Biochem Biophys Res Commun. 2006; 347:1048–1052. [PubMed: 16857171]
41. Nowak E, Etienne O, Millet P, Lages CS, Mathieu C, Mouthon MA, Boussin FD. Radiation-induced H2AX phosphorylation and neural precursor apoptosis in the developing brain of mice. Radiat Res. 2006; 165:155–164. [PubMed: 16435914]
42. Löbrich M, Rief N, Kühne M, Heckmann M, Fleckenstein J, Rübe C, Uder M. In vivo formation and repair of DNA double-strand breaks after computed tomography examinations. Proc Natl Acad Sci USA. 2005; 102:8984–8989. [PubMed: 15956203]
43. Banáth JP, MacPhail SH, Olive PL. Radiation sensitivity, H2AX phosphorylation, and kinetics of repair of DNA strand breaks in irradiated cervical cancer cell lines. Cancer Res. 2004; 64:7144–7149. [PubMed: 15466212]
44. Rothkamm K, Balroop S, Shekhdar J, Fernie P, Goh V. Leukocyte DNA damage after multi-detector row CT: A quantitative biomarker of low-level radiation exposure. Radiology. 2007; 242:244–251. [PubMed: 17185671]

45. Kee N, Sivalingam S, Boonstra R, Wojtowicz JM. The utility of ki-67 and BrdU as proliferative markers of adult neurogenesis. J Neurosci Methods. 2002; 115:97–105. [PubMed: 11897369]
46. Mizumatsu S, Monje ML, Morhardt DR, Rola R, Palmer TD, Fike JR. Extreme sensitivity of adult neurogenesis to low doses of X-irradiation. Cancer Res. 2003; 63:4021–4027. [PubMed: 12874001]
47. Ma DK, Jang MH, Guo JU, Kitabatake Y, Chang ML, Pow-Anpongkul N, Flavell RA, Lu B, Ming GL, Song H. Neuronal activity-induced Gadd45b promotes epigenetic DNA demethylation and adult neurogenesis. Science. 2009; 323:1074–1077. [PubMed: 19119186]
48. Chehrehasa F, Meedeniya ACB, Dwyer P, Abrahamsen G, Mackay-Sim A. EdU, a new thymidine analogue for labelling proliferating cells in the nervous system. J Neurosci Methods. 2009; 177:122–130. [PubMed: 18996411]
49. Ge S, Goh ELK, Sailor KA, Kitabatake Y, Ming GL, Song H. GABA regulates synaptic integration of newly generated neurons in the adult brain. Nature. 2006; 439:589–593. [PubMed: 16341203]
50. Tryggestad E, Armour M, Iordachita I, Verhaegen F, Wong JW. A comprehensive system for dosimetric commissioning and Monte Carlo validation for the small animal radiation research platform. Phys Med Biol. 2009; 54:5341–5357. [PubMed: 19687532]
51. Hopewell JW, Cavanagh JB. Effects of X irradiation on the mitotic activity of the subependymal plate of rats. Br J Radiol. 1972; 45:461–465. [PubMed: 5029031]
52. Tada E, Parent JM, Lowenstein DH, Fike JR. X-irradiation causes a prolonged reduction in cell proliferation in the dentate gyrus of adult rats. Neuroscience. 2000; 99:33–41. [PubMed: 10924950]
53. Monje ML, Toda H, Palmer TD. Inflammatory blockade restores adult hippocampal neurogenesis. Science. 2003; 302:1760–1765. [PubMed: 14615545]
54. Rola R, Otsuka S, Obenaus A, Nelson GA, Limoli CL, VandenBerg SR, Fike JR. Indicators of hippocampal neurogenesis are altered by ^{56}Fe-particle irradiation in a dose-dependent manner. Radiat Res. 2004; 162:442–446. [PubMed: 15447038]
55. Rola R, Fishman K, Baure J, Rosi S, Lamborn KR, Obenaus A, Nelson GA, Fike JR. Hippocampal neurogenesis and neuroinflammation after cranial irradiation with 56Fe particles. Radiat Res. 2008; 169:626–632. [PubMed: 18494546]
56. Snyder JS, Hong NS, McDonald RJ, Wojtowicz JM. A role for adult neurogenesis in spatial long-term memory. Neuroscience. 2005; 130:843–852. [PubMed: 15652983]
57. Tada E, Parent JM, Lowenstein DH, Fike JR. X-irradiation causes a prolonged reduction in cell proliferation in the dentate gyrus of adult rats. Neuroscience. 2000; 99:33–41. [PubMed: 10924950]
58. Kaplan MS, Bell DH. Mitotic neuroblasts in the 9-day-old and 11-month-old rodent hippocampus. J Neurosci. 1984; 4:1429–1441. [PubMed: 6726341]
59. Gage FH, Kempermann G, Palmer TD, Peterson DA, Ray J. Multipotent progenitor cells in the adult dentate gyrus. J Neurobiol. 1998; 36:249–266. [PubMed: 9712308]
60. Cameron HA, Mckay RDG. Adult neurogenesis produces a large pool of new granule cells in the dentate gyrus. J Comp Neurol. 2001; 435:406–417. [PubMed: 11406822]
61. Suzuki K, Okada H, Yamauchi M, Oka Y, Kodama S, Watanabe M. Qualitative and quantitative analysis of phosphorylated ATM foci induced by low-dose ionizing radiation. Radiat Res. 2006; 165:499–504. [PubMed: 16669703]

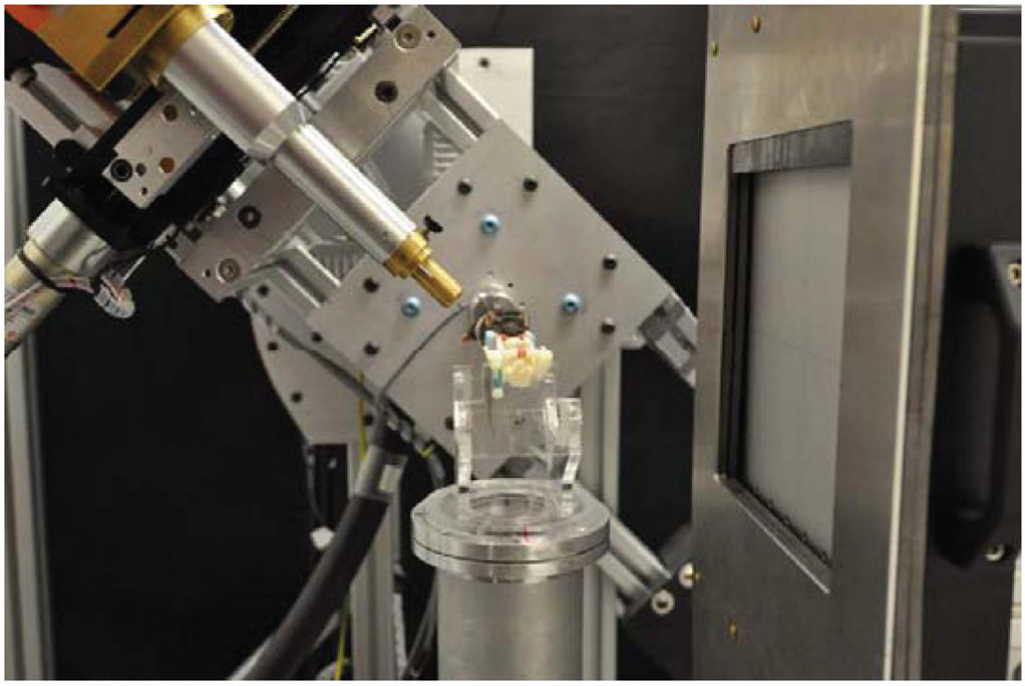

FIG. 1.
The small animal radiation research platform (SARRP) showing the X-ray tube (upper left), the collimating nozzle, the robotically controlled stage (center) and the flat-panel X-ray imager (right). Here the gantry angle is set at 45° from the vertical.

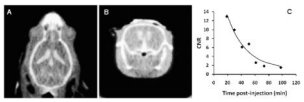

FIG. 2.

Intrathecal injection of iodine in the cisterna magna results in high-contrast signal in the ventricles on CT scans acquired on the SARRP device in the axial (panel A) and coronal (panel B) planes. Attenuation of intrathecal contrast is quantified in terms of contrast-to-noise ratio (CNR) in the CT scans (panel C).

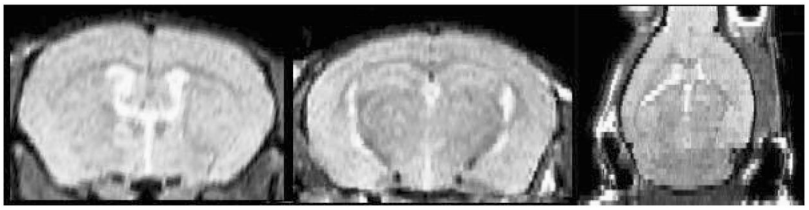

FIG. 3.
MRI images of the rostral aspect of the lateral ventricle (left), the hippocampus (middle) and a reconstructed axial cut at the ventricle level (right). Images are T2-weighted acquired on a 9.4 T MR unit.

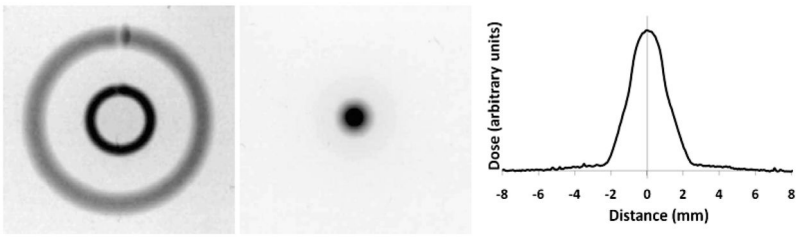

FIG. 4.

Film dosimetry from a treatment with arcs at two different gantry angles of 30° and 60° off vertical. Film from the top phantom layer (left panel) shows the two arcs, while the two arcs converge to a single point on the center film layer (center panel). The FWHM of the profile through the center film is 2.31 mm (right panel).

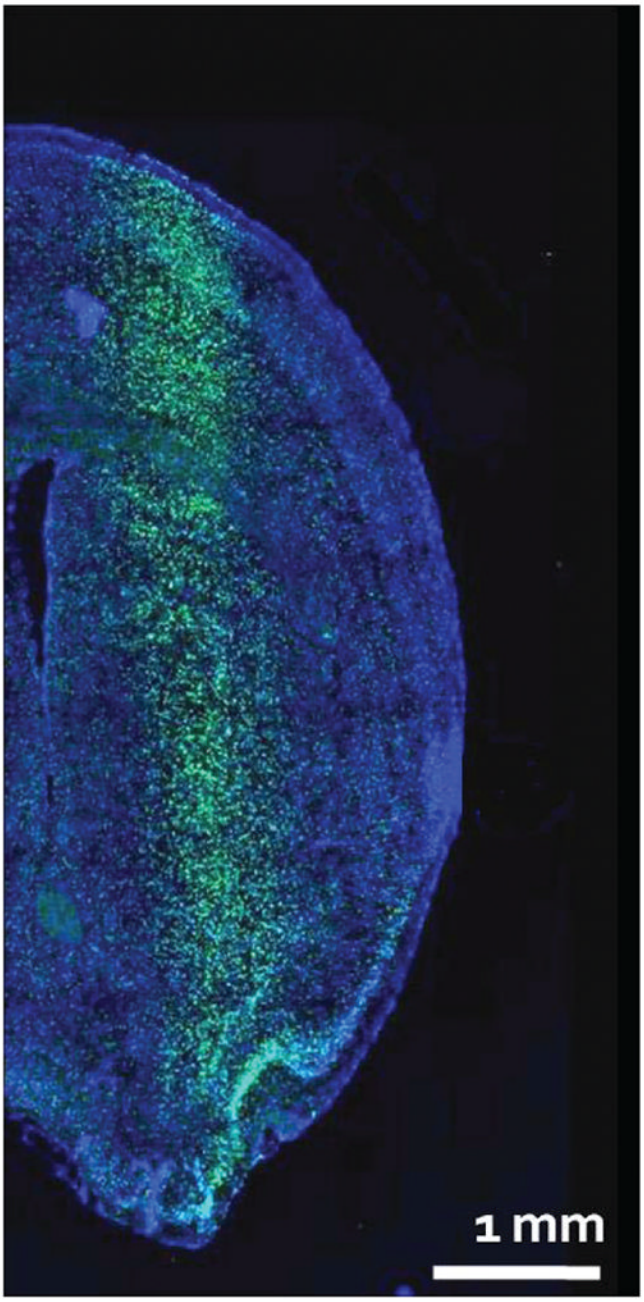

FIG. 5.
γ-H2AX-stained section from a mouse brain that received 10 Gy through a 1-mm-diameter beam. Stains are γ-H2HX (green) and DAPI (blue).

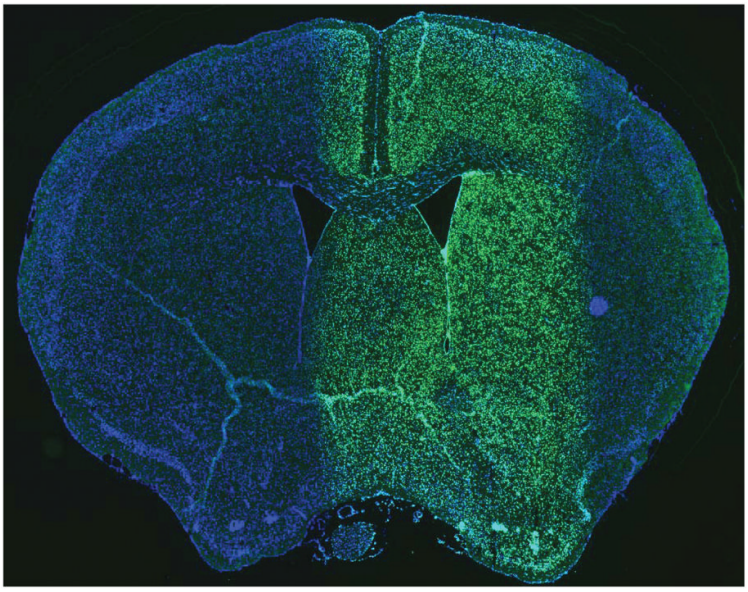

FIG. 6.
γ-H2AX-stained section from a mouse brain that received 10 Gy through a 3 × 3 mm square beam. The intended target was the lateral wall of the right lateral ventricle.

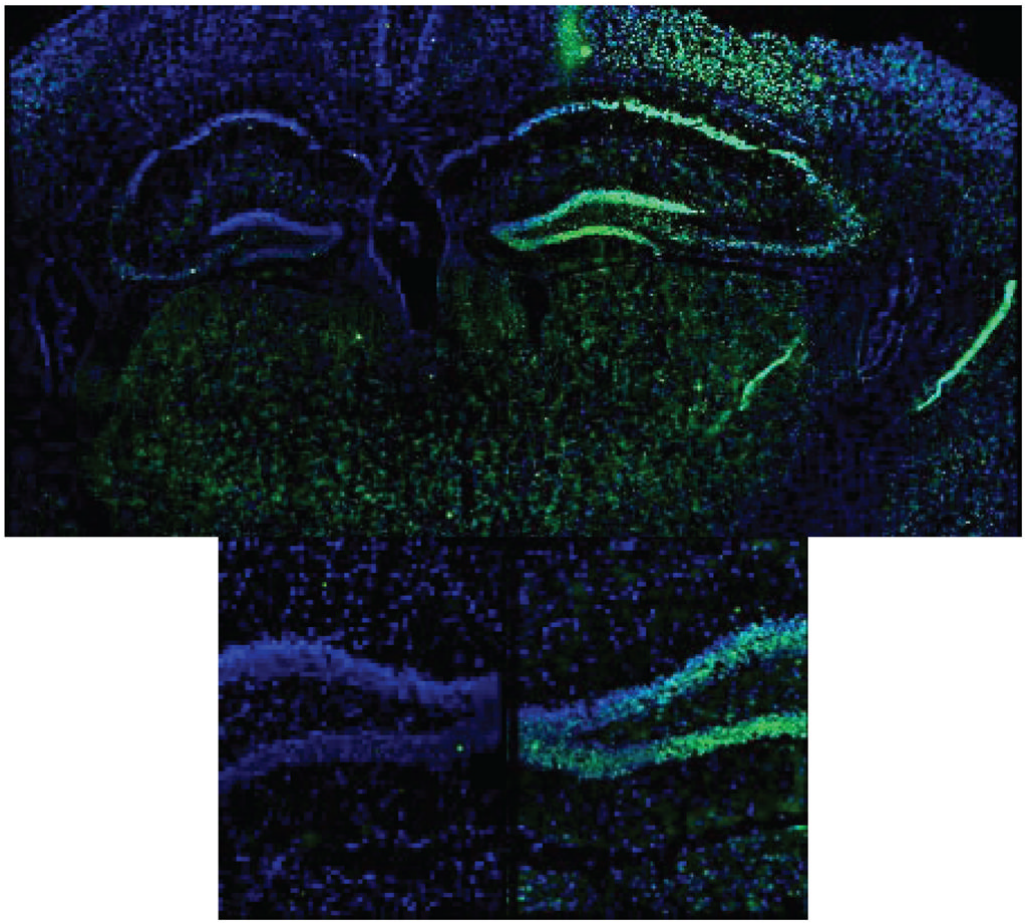

FIG. 7.
γ-H2AX-stained section from a mouse brain that received 10 Gy arc treatment delivered to the right hippocampus.

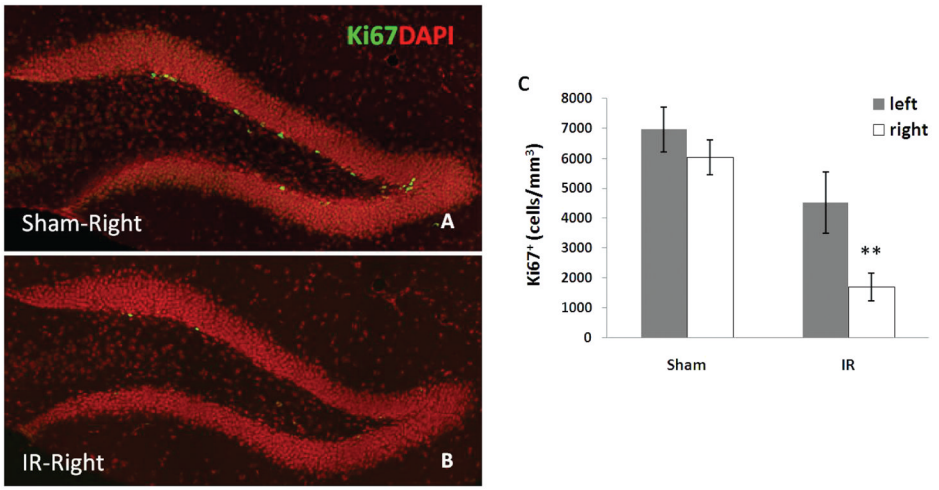

FIG. 8.

Dentate gyrus of the hippocampus 24 h postirradiation stained for Ki-67 (green) and DAPI (red). Sections from a mouse receiving no radiation (panel A) and 10 Gy radiation localized to the right hippocampus (panel B). Panel C: Ki67 quantification. $^{**}P \leq 0.001$ with respect to the mice receiving no radiation. Differences in the unirradiated (left) side in the sham-irradiated and irradiated (IR) mouse are not significant ($P = 0.11$) nor are the differences between the unirradiated (left) and irradiated (right) in the irradiated mouse ($P = 0.06$).

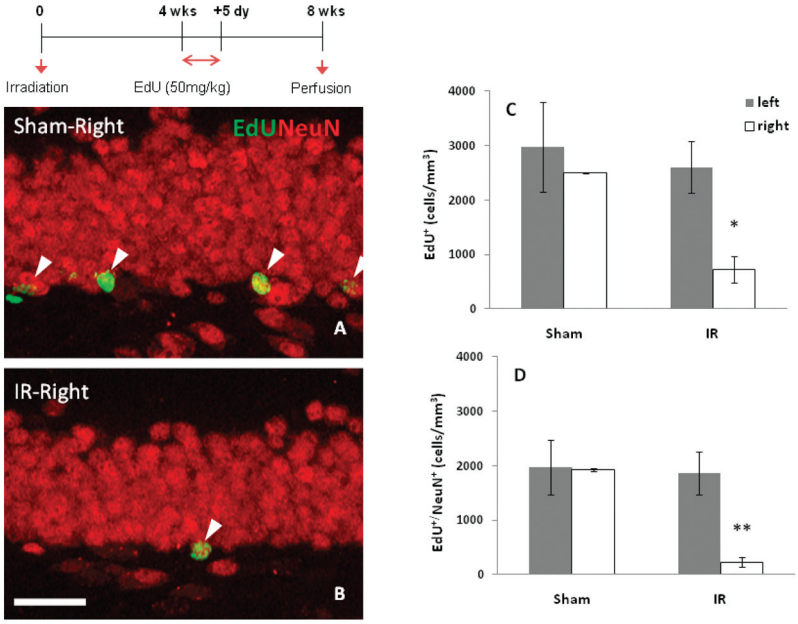

FIG. 9.

Neurogenesis in the dentate gyrus of the hippocampus 8 weeks after localized irradiation. Histology sections from a mouse receiving no radiation (panel A) and mouse receiving 10 Gy localized to the right hippocampus (panel B) with staining for EdU injected 4 weeks after irradiation (IR) and NeuN, a marker for mature neurons. The scale bar indicates a size of 50 μm. The number of EdU^+ cells (panel C) and the number of $EdU^+/NeuN^+$ cells (panel D) on the unirradiated (left) and irradiated (right) side. $^{**}P \leq 0.00$, $^{*}P \leq 0.05$ compared to the mice receiving no radiation.

TABLE 1

Stereology Data for Hippocampus Neurogenesis Experiments

	Ki-67				EdU				EdU/NeuN			
	Unirradiated		Irradiated		Unirradiated		Irradiated		Unirradiated		Irradiated	
	Left	Right	Left	Right	Left	Right	Left	Right	Left	Right	Left	Right
	7982	5635	6228	1799	4624	2491	3197	317	2966	1928	1912	125
	5739	7250	5913	2924	2198	2490	1673	1141	1401	1961	1145	405
	8459	6595	1727	1378	2095	2514	2944	723	1544	1873	2511	153
	5648	4637	4208	665								
Mean	6957	6029	4519	1692	2972	2498	2605	727	1970	1921	1856	228
SEM	839	469	1451	461	826	8	472	238	500	26	395	89

Notes. Ki-67 staining 24 h after irradiation (left portion), EdU labeling (middle portion) and EdU/NeuN double labeling (right portion), 8 weeks after irradiation. Radiation (10 Gy)was delivered to the right hippocampus. All numbers are cells/mm^3.

Radiat Res. Author manuscript; available in PMC 2012 June 1.